Identification of the Cold Pool Phenomenon at Soekarno-Hatta Airport Site

Soni Soeharsono[1*], Nurjanna Joko Trilaksono[2]

[1,2]Department of Meteorology, Faculty of Earth Sciences and Technology, Institut Teknologi Bandung, Jl. Ganesha No. 10, Bandung 40132, West Java, Indonesia

[*]soni.soeharsono@bmkg.go.id

Abstract: *The cold pool phenomena over Soekarno-Hatta International Airport (6.16°S, 106.64°E), which are known to pose significant hazards to aviation operations, particularly during take-off and landing. Multi-instrument datasets were analysed, including minute-resolution surface meteorological observations, Doppler radar imagery, and wind profiler measurements up to 3 km altitude. The aim was to document the thermodynamic and characteristics signatures of cold pools and to evaluate their potential detection using machine learning techniques. Results show that cold pools are consistently associated with sharp wind direction shifts of more than 60°, sudden increases in wind speed ranging from 11 to 22 knots, and rapid surface temperature potential (θ) drops of about 2.0–6.0 K. Radar reflectivity data reveal strong gradients at the edge of convective cells, which correspond to severe thunderstorm signatures. These features were highlighted by a Convolutional Neural Network (CNN) and Grad-CAM analysis, confirming that reflectivity gradients are the primary indicators used by the model to identify gusty wind events. Vertical profiles derived from the wind profiler indicate cold pool depths between 300 and 1450 m, propagation speeds from 1.5 to 16.1 m/s, and strength values (C^2) exceeding 130 m^2/s^2 in certain cases. Moreover, an increase in relative humidity of up to 30% was observed at the cold pool boundaries, supporting the initiation of new convective clouds with lower cloud bases. These findings highlight that cold pools are not only critical aviation hazards due to surface wind gusts but also play a key role in sustaining convective development in the airport environment. The combined use of multi-instrument observations and machine learning provides a robust framework for cold pool identification, offering both physical consistency and operational potential. The approach presented here demonstrates that adaptive early-warning systems for airports could be developed based on integrated observational data and artificial intelligence. Such systems would improve safety margins and operational efficiency by anticipating hazardous cold pool events before they impact aircraft during landing phases.*

Keywords: Cold pool, Gusts, Convective clouds, Wind profiler

Introduction

Air transportation activities using aircraft are crucial, and their need for international regulations governing safe and efficient operational processes. Safety in aviation relates to the take-off and landing process from the departure airport to the destination airport or an alternate airport. Efficiency is directly related to the efficient use of fuel during the safe flight process. Certain meteorological phenomena can hinder safe and efficient flight operations.

On April 5th, 2022, April 16th, 2022 and April 27th, 2022, meteorological phenomena affected the tailwind of aircraft during landing, forcing them to perform a go-around maneuver and touch down on the other side of the runway. This, of course, impacted the fuel efficiency of the aircraft. The aircraft's approach altitude on the airport runway was 1500 feet above the 3 nm from touch-down zone, apparently not safe enough for aircraft still experiencing its impact.

This raises the question for the author to conduct a study on how high the height of phenomena produced by severe thunderstorms such as microbursts, gusts, and gust fronts can impact the Soekarno-Hatta airport area, for aircraft during the take-off and landing phases. In this study, the author will only conduct a study to identify gust front or cold pool phenomena detected above the Soekarno-Hatta airport area that have a significant impact on flight operations.

Severe thunderstorms that occur in airport areas or in the airport vicinity can produce phenomena such as microbursts and gust fronts (cold pools) that impact aircraft take-off and landing activities at the aerodrome. Cold pools are produced by various storm morphologies, including supercell thunderstorms and multicellular storms/clusters, The leading edge of the cold pool (LECP) is likely associated with intense wind gusts, posing a severe threat to aircraft, they represent a severe hazard for aviation as the LECP is likely to be associated with intense wind (Borque et al., 2020).

Shi et al. (2019) conducted severe thunderstorm research using a radar signature weak echo region with a tight low level reflectivity gradient. The weak echo region (WER) is a region with low radar reflectivity that is bounded on one side and above by strong echoes. It is usually located on the low-altitude inflow side of a thunderstorm. The WER is caused by a strong updraft that carries precipitation particles to the middle levels before they grow to a radar-detectable size. The strong tilted echo above WER is called overhang echo (Lemon & Doswell, 1979; Shi et al., 2019).

McDonald and Weiss (2021) conducted a study using virtual potential temperature (θ_v) as a variable to quantify the magnitude of the cold pool. This study considers observed temporal θ_v gradients to be baroclinic regions, and uses their magnitude as a proxy for potential baroclinic vorticity generation. Stronger gradients can lead to larger baroclinic vorticity generation, radar reflectivity gradient was used as a proxy for the θ_v gradient. However, this method is still subjective, resulting in errors in gradient calculations that cannot be fully measured. In this study, the author aims to quantify the radar signature gradient reflectivity in a case study of a severe thunderstorm phenomenon.

Identification using only radar signatures to identify cold pools in research has several shortcomings, as severe thunderstorms not only produce cold pools but also produce other strong wind phenomena, as mentioned in the opening paragraph. Several studies related to cold pools have used various remote sensing methods, such as weather satellites and doppler radar, to detect these phenomena, but these have weaknesses.

Allen et al. (2013); Bou Karam et al. (2014); Marsham et al. (2013) investigated cold pool events and dust emissions over west and northwest Africa using infrared satellite imagery from the Meteosat Spinning Enhanced Visible and Infrared Imager (SEVIRI) and Lensky and Rosenfeld (2008), which utilizes a red-green-blue (RGB) composite of three infrared bands.

Its high spatiotemporal resolution (15 minutes, 0.03°) allows it to reveal the leading edge of the cold pool through dust emission. The disadvantage is that when high clouds are present, dust cannot be seen, making it difficult to distinguish between the deep convection that can produce the cold pool and other high-level clouds. Ashpole and Washington (2013); Kocha et al. (2013) noted that because cold pools originate from deep convection, which is usually surrounded by extensive high-level cloud cover, they can be anticipated by relying on infrared imagery (Redl et al., 2015).

Zheng et al. (2014) stated that the condition of the cloud-covered area and accompanied by precipitation results in a bias for the visibility of the cold pool, making it difficult to distinguish between the cold pool and its background. The application of image segmentation methods based on edges and constrained regions is less effective in detecting cold pools. Another limitation of the method related to identifying cold pools using doppler radar is that a cold pool may intersect with other weak narrow band echoes, and in such cases, the interference can be ignored. In addition, a cold pool shows the presence of wind shear or convergence lines in the

velocity field, but the recognition of wind shear or convergence lines often fails because the doppler radial velocity field is of low quality (Yuan et al., 2018). Based on the shortcomings of the method in detecting the cold pool phenomenon using that remote sensing observation method, the author intends to identify this phenomenon using another remote sensing observation methods, such as radar wind profilers.

Literature Review

Mallinson and Lasher-Trapp (2019) defined a cold pool as a parcel of air at the surface with potential temperature perturbation less than or equal to -2 K. They noted that a less stringent threshold of -1 K led to noisy fields, while more stringent thresholds (≤ - 4 K) did not significantly alter results. The onset of cold pools in their simulations was identified by the appearance of a -2 K surface potential temperature perturbation. James et al. (2006); Ross and Lasher-Trapp (2024) similarly defined cold pools in their simulations as a contiguous area with a potential temperature perturbation threshold of -1 K at the lowest model level (100 m) from the horizontally homogeneous environment. They also used this -1 K perturbation to identify the first appearance of a cold pool at the ground.

Redl et al. (2015), in an objective detection method for cold pool events, included a criterion for a decrease in temperature of 1.5–2.5 K in less than 30 minutes at the leading edge of a cold pool. Borque et al. (2020) observed temperature decreases ranging from 2°C to 6°C at surface stations as the leading edge of a cold pool passed. Falk and Van Den Heever (2023) studied the impact of "initial temperature deficits" of cold pools, noting that observed cold pools can have deficits from 1 K or less in moist maritime environments to up to 17 K in drier continental environments. Tompkins (2001) used a buoyancy threshold of $B = -0.005\ m^2s^{-1}$ to identify cold pool air, noting that buoyancy and temperature structure were similar.

The passage of a cold pool's leading edge is characteristically associated with an increase in wind speed, often described as intense wind gusts (Borque et al., 2020; Redl et al., 2015). Observations from Oklahoma Mesonet stations, for example, recorded wind speeds that almost doubled at one location (from approximately 4 m/s to over 10 m/s) and increased significantly at others upon the cold pool's passage (Borque et al., 2020). Similarly, simulated cold pools have shown wind enhancement matching observations, with wind increasing ahead of the rain, indicating the cold pool outflow (Li et al., 2014). The difference between the wind averaged

within the cold pool boundary and the domain-averaged wind defines the cold pool expansion rate, highlighting this change in wind (Li et al., 2014).

A shift in the low-level flow is also a key characteristic of a cold pool's passage. In one observed case, the prevailing undisturbed wind, initially from the northeast, shifted to the southeast or east after the leading edge of the cold pool moved through. This wind shift is consistent with what is expected given the orientation and outward propagation of the cold pool's leading edge (Borque et al., 2020). Within a persistent mountain valley cold pool, a transition from westerly flow aloft to a weak easterly component has also been observed (Billings et al., 2006).

Cold pools create conditions conducive to the initiation of *new* convection with potentially lower cloud bases at their leading edge (Borque et al., 2020; Li et al., 2014; Mallinson & Lasher-Trapp, 2019; Redl et al., 2015; Ross & Lasher-Trapp, 2024; Tompkins, 2001). The leading edge of the cold pool forcibly lifts potentially buoyant environmental air up and over its boundary, enabling it to reach its Level of Free Convection (LFC) (Falk & Van Den Heever, 2023; Li et al., 2014; Ross & Lasher-Trapp, 2024; Tompkins, 2001). This dynamic lifting facilitates the formation of new convective clouds.

Cold pools, particularly at their edges, can increase the water vapor mixing ratio in the atmosphere (Falk & Van Den Heever, 2023; Tompkins, 2001). This increase in moisture can lower the Lifting Condensation Level (LCL) and the LFC (Falk & Van Den Heever, 2023; Tompkins, 2001). A lower LCL means that air parcels need to be lifted less to become saturated and form a cloud, thus enabling new clouds to form at lower altitudes. Simulated moist zones are created at the cold pool heads, which are advected horizontally and do not diminish as rapidly as vertical velocity, contributing to sustained moistening (Falk & Van Den Heever, 2023; Li et al., 2014).

Mallinson and Lasher-Trapp (2019); Ross and Lasher-Trapp (2024) note that while the leading edge of a cold pool is favourable for new convection, the area behind the gust front tends to be stabilized, which can suppress the initiation of new convection. Therefore, the effect on cloud base height is primarily localized to the cold pool's leading edge and is associated with the formation of new clouds rather than a general lowering of existing cloud bases across the entire affected region.

Methodology

The method used in this study to identify the cold pool phenomenon is a quantitative descriptive method. Surface meteorological observation data were collected using an automatic weather observing station from the meteorological observation authority site at Soekarno-Hatta Airport, which is equipped with complete equipment including wind vector and scalar observations, lidar ceilometers, temperature, pressure, and humidity. Initial identification of the cold pool phenomenon using surface observation data is highly reliable because the observation data is sufficiently dense to record minute-by-minute changes.

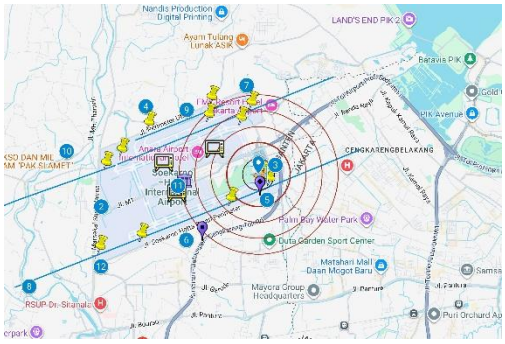

Figure 1: Soekarno-Hatta Airport site.

Cold pools are identified using changes in wind direction and speed. Identification uses changes or deviations in wind direction of ≥ 60°. This provision is in accordance with the aviation convention for wind changes in airport weather reporting that significantly impact aircraft take-off and landing operations on the runway. This change in wind direction is also useful in identifying the source of wind phenomena originating from the cardinal direction, the conformity of this wind direction with the position of convective clouds confirms one thing related to the suspect or not convective clouds.

Changes in wind speed to identify cold pools with a magnitude change of at least 10 knots recorded on the instrument, accompanying changes in wind deviation in accordance with the provisions of the aviation convention for significant weather. In this paper, the wind speed data used is minutely observation data that records changes that include gusts.

Air temperature measured at the same site was used to identify cold pools through changes in air temperature values. In this paper, the authors used a threshold of -2°C air temperature decrease. This decrease in air temperature was deemed significant based on research Borque et al. (2020); Redl et al. (2015). Cold pools were also identified by potential temperature perturbations of less than -2 K. A temperature decrease of less than -2 K was considered a

suspect cold pool phenomenon that passed through the surface observation sensor site at Soekarno-Hatta.

Surface meteorological observations at the Soekarno-Hatta site were equipped with a cloud base height observation sensor with a lidar ceilometer. This sensor monitors the height of low, middle, and high cloud bases. The low cloud base height data used, with recorded changes in altitude, showed a decrease of 500 feet. The identified suspects fall into the cold pool phenomenon category, which occurs when the cloud base height decreases over a short period of time. These changes in meteorological conditions were measured over an observation period of less than 30 minutes, as applied by Redl et al. (2015).

The suspected timing of the cold pool event identified through surface meteorological observations was confirmed with C-band single-polarization (6.16S, 106.64E) and X-band dual-polarization (6.118S, 106.67E) doppler radar. Radar reflectivity images captured the echoes of convective clouds detected producing the cold pool, at times before and after the cold pool was detected in surface meteorological observations. The aftermath of the cold pool event was analysed to strengthen evidence that the cold pool initiated the formation of new convective clouds.

The generated doppler radar reflectivity images of suspected cold pool events (January 2022 – May 2025) from the analysis of surface meteorological data with an automated weather observing system, it was analyzed along with radar image data from the date of the case study (2011 – 2024) from the flight observation data report (e.g. METAR, Met Report, SPECI and SPECIAL report) which included wind gust reports were collected., along with radar reflectivity images of clear weather events (e.g. sea breeze), will be analyzed using a CNN machine learning model.

More than 1200 column maximum (CMAX) radar images were collected and processed with CNN to produce model output with Hierarchical Data Format version 5 (HDF5 or h5) and NumPy Zip archive (NPZ) extensions. The model output from this CNN will be used as input for Grad-CAM to quantify weak echo regions or low-level tight gradient reflectivity. The Convolutional Neural Network (CNN) and Grad-CAM model method identifies gradient values by leveraging the inherent structure of CNNs and applying a gradient-based localization technique to provide visual explanations for model decisions (Chen et al., 2022; Selvaraju et al., 2020).

CNNs are deep learning models widely used in computer vision tasks for automatic feature extraction, they consist of multiple layers, including convolutional layers and pooling layers. Convolutional Layers extract local patterns and higher-level visual constructs from the input image. Deeper convolutional layers capture more semantic information while retaining spatial details (Selvaraju et al., 2020; Tang et al., 2021). The output of a convolutional layer is a set of feature maps, where each map highlights specific features learned by the network (Tang et al., 2021). Pooling Layers reduce the dimensionality of the feature maps, making the feature extraction more robust and reducing computational costs (Tang et al., 2021).

Grad-CAM's Use of Gradients for Localization, Grad-CAM (Gradient-weighted Class Activation Mapping) is a technique that makes CNN-based models more transparent and explainable by producing 'visual explanations'. It specifically uses gradient information to highlight the important regions in an image that contribute to a particular decision by the CNN (Selvaraju et al., 2020).

To quantify the cold pool phenomenon at the Soekarno-Hatta meteorological authority observation site with remote sensing using radar wind profiler data (6.118S, 106.679E). The author uses this radar wind profiler observation data, it has advantages in detecting cold pool phenomena because it has atmospheric column sample observations up to 3000 meters and the atmospheric sampling time is repeated every 5 minutes, so that when a suspected cold pool passes the observation point of this site it will be captured well.

The raw wind profiler data is processed in such a way as to produce secondary data such as wind direction and speed, wind shear, vertical velocity, precipitation, virtual temperature and temperature gradient observations every 5 minutes, sampling every 100 meters to the peak observation height of 3000 meters. The calculation of potential temperature involves surface observation data including dry bulb temperature, QNH, then the surface pressure data of the station at an altitude of 11 meters msl and pressure data every 100 meters are obtained using the pressure formula with QNH reference data. Dry bulb temperature data per 100 meters uses surface dry bulb temperature observations calculated by the wind profiler temperature gradient. The calculation of potential temperature (θ) to obtain the cold pool strength (C^2) and cold pool propagation (C) values uses the formula from Weisman (1992), but in this study only at single observation site point;

$$B = g\left(\frac{\theta_p - \theta_{p0}}{\theta_{p0}}\right) \quad (1)$$

$$C^2 = 2g\int_0^H (-B)dz \quad (2)$$

$$\theta_{(z)} = T_{(z)}\left(\frac{p_0}{p_{(z)}}\right)^{\frac{R_d}{C_p}} \quad (3)$$

Where H is the depth of the cold pool from the buoyancy value (B) using a threshold of ≤ 0 m^2s^{-1} and a value of ≤ -0.005 m^2s^{-1} which is identified as a suspected cold pool from the results of radar wind profiler calculations, (a value of -0.005 m^2s^{-1} ≤ B ≤ 0 m^2s^{-1} is not counted as a suspected cold pool).

Results and Discussions

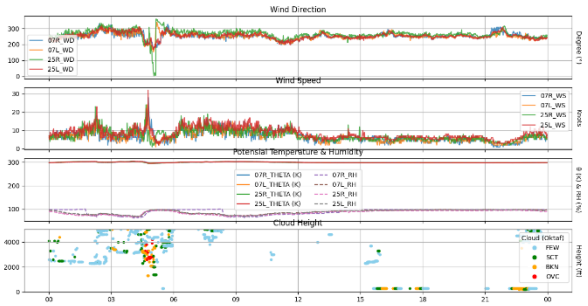

Figure 2: Surface meteorological observation data of vector and scalar winds, potential temperature, humidity, number and height of cloud bases.

This image shows (fig.2) the wind dynamics, potential temperature, humidity, and cloud base number and height during a cold pool event. The sharp change in wind direction, accompanied by an increase in wind speed and a decrease in potential temperature, indicates a cold air mass moving over the observation area. A decrease in cloud base height is also observed after the cold pool propagation, consistent with the theory that cold air from a downdraft can trigger the formation of new clouds with lower bases. This surface observation data analysis was carried out with the availability of well-documented data from January 2022 until May 2025 and successfully obtained the same pattern as the pattern in fig. 2 (44 cases not shown), such as significant changes in wind direction and speed, spikes in humidity, decreases in air temperature and potential temperature and decreases in cloud base height as many as 45 cases including in pilot report news such as April 5th, 2022, April 16th, 2022 and April 27th, 2022 which caused the aircraft to fail to landing and had to perform a go-around maneuver.

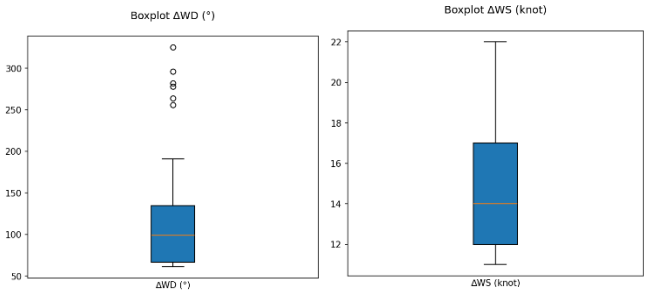

Figure 3: Boxplot of wind direction deviation (left) and delta wind speed of suspected cold pool (right).

The boxplot results show a minimum wind direction deviation of 61° and a maximum of 325° (analysed clockwise), with a median of approximately 99° (fig. 3 left). These values confirm that the cold pool is characterized by significant changes in wind direction, as standardized by aviation meteorological conventions. Meanwhile, wind speed changes ranged from 11 to 22 knots, with a median of 14 knots (fig. 3 right). These large speed changes clearly represent a potential hazard to flight operations, particularly during the landing phase.

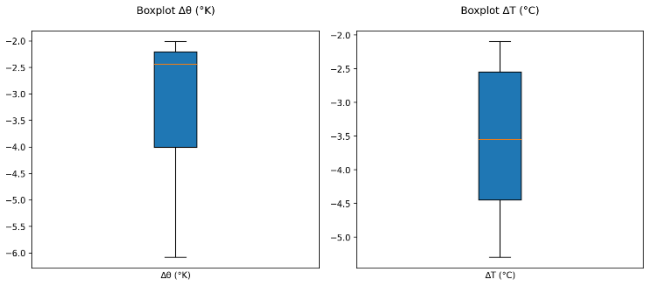

Figure 4: Boxplot of delta temperature potential Δθ (left) and delta air temperature ΔT (right).

The cold pool was identified by a potential temperature (θ) drop of -6.08 K (minimum), with a median (Q2) of -2.45 K and max -2.0 K (fig. 4 left), and an air temperature drop of -5.3°C (min) with a median (Q2) of -3.55°C, and max -2.1°C (fig. 4 right). These values reinforce the evidence that cold air resulting from precipitation evaporation rapidly lowers temperatures. This condition meets the criteria for a temperature drop of ≥ 2°C in a short period of time, a strong indicator of a cold pool.

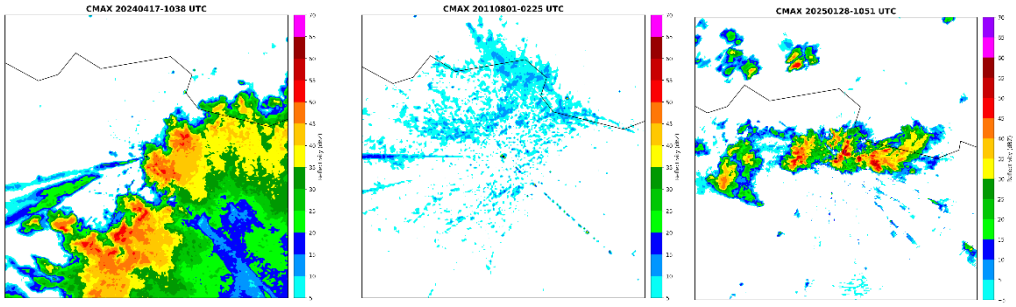

Figure 5: CMAX reflectivity of single polarization C-band doppler radar (left), dual polarization X-band doppler radar (right) and C-band of sea breeze case (middle).

Radar images show a convective cell with high reflectivity values and a strong reflectivity gradient radar signature associated with gusty winds. C-band radar displays a broad area of strong reflection (fig. 5 left), while dual-polarization X-band radar reveals more detailed structure, the clouds triggered by the cold pool phenomenon which occurred on January 28th, 2025 (fig. 5 right), which caused flooding around Soekarno-Hatta Airport, including a sharp reflectivity gradient at the edge of the storm cell. This feature is consistent with the location of the gust front.

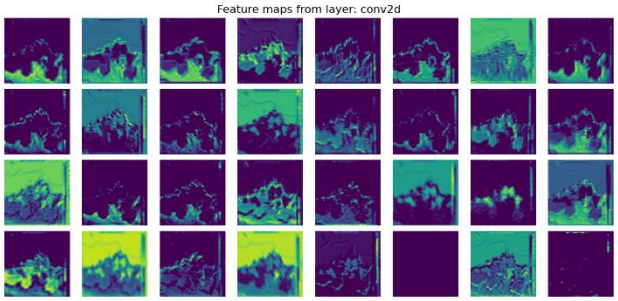

Figure 6: CNN model extract.

A CNN model was used to recognize the distinctive pattern of cold pools in radar imagery. The extraction results showed that the network was able to identify areas of low-high reflectivity gradients as the primary feature of cold pools. This provided the basis for further analysis using Grad-CAM (fig. 6).

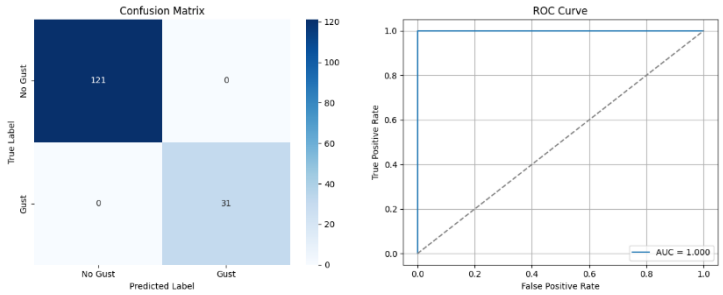

(a)

(b)

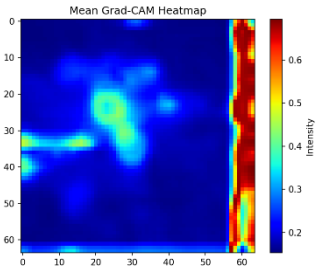

(c)

Figure 7: Results of CNN confussion metrix (a), ROC curve (b) and Grad-CAM heatmap (c).

The confusion matrix demonstrated good classification performance (fig. 7a), reinforced by a ROC curve with a near-perfect AUC value (fig. 7b). The Grad-CAM heatmap shows the model's focus on the edges of convective clouds, precisely in the reflectivity gradient area associated with gusty winds. This finding aligns with the physical understanding that the cold pool edge is the most dangerous zone for aviation activity (fig. 7c).

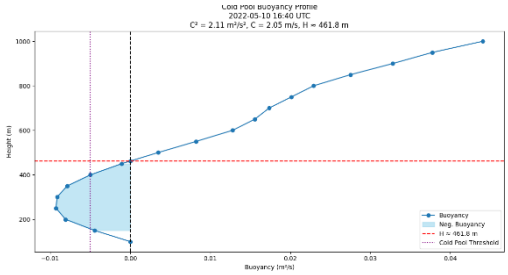

Figure 8: Cold pool vertical profile.

The vertical profile illustrates the distribution of buoyancy, the height of the cold pool, the strength of the cold pool, and the speed of the cold pool's propagation in the atmospheric column. The cold pool appears to extend to a certain height with a clear top. This indicates that the observed phenomenon is not simply a surface fluctuation, but rather extends to a layer several hundred meters above the surface (fig. 8).

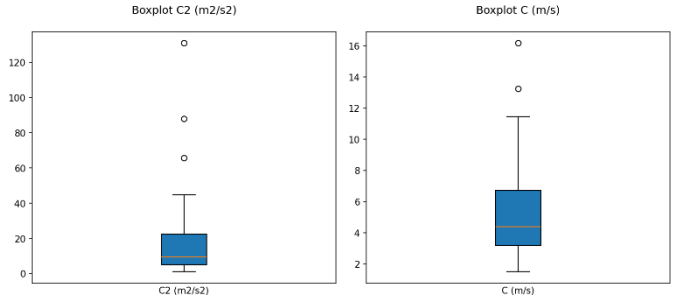

Figure 9: Boxplot of cold pool strength (left) and cold pool propagation speed magnitude (right).

Magnitudes of cold pool strength or C^2 values ranged from 1.13 to 130.9 m^2/s^2, with a median of 9.66 m^2/s^2 (fig. 9 left), indicating significant strength variation between events. Cold pool propagation velocities were recorded between 1.5 and 16.18 m/s, with a median of 4.4 m/s (fig. 9 right). This value is consistent with previous studies by Tompkins (2001) that suggest cold pool propagation is generally in the range of 5–10 m/s, strong enough to trigger significant disturbances in the local atmospheric environment.

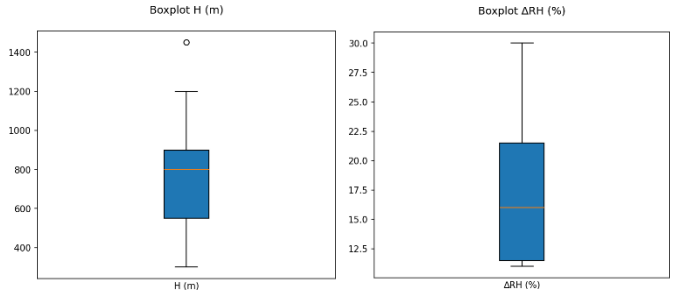

Figure 10: Boxplot of cold pool height, (left) humidity surges (right).

The cold pool depth was detected between 300–1450 m, with a median of 800 m (fig. 10 left), indicating that this phenomenon can reach the entire approach area of the aircraft when landing. Meanwhile, relative humidity increased significantly, with a median of 16% and a maximum of 30% (fig. 11 right). This increased humidity supports new cloud formation at the edge of the cold pool, potentially extending the lifespan of the convective system.

The results of the Grad-CAM analysis applied to the CNN model show that the area's most frequently highlighted by the model are around the edges of high-reflectivity structures in the CMAX radar imagery. This pattern is consistently observed across the cases analysed, suggesting a link between areas with sharp reflectivity gradients and gusty wind events at the surface.

The Grad-CAM analysis of CMAX imagery indicates that the CNN model consistently focuses on the area surrounding the center of maximum reflectivity. The average Grad-CAM focus score at a 1-km radius was recorded at 0.5665 and remained relatively stable at 2-km (0.5660) and 3-km (0.5666) radii. A slight decrease began to be observed at a 5-km radius with a value of 0.5618, indicating that the area outside the storm core was contributing less to the model's decisions. This finding indicates that the model is placing greater emphasis on the convective core and its surrounding regions, consistent with the physical understanding that gusty wind events are generally triggered by strong convective activity in the storm core and a tight reflectivity gradient around it. Therefore, the high consistency of focus scores at the core radius supports the interpretation that the CNN successfully identified radar signatures relevant for detecting potential gusty wind events.

Conclusion

This research successfully identified the characteristics of the cold pool phenomenon occurring in the Soekarno-Hatta Airport area using surface meteorological observation data, C-band and X-band doppler radar, and wind profiler radar. The analysis showed that the cold pool was characterized by a significant change in wind direction ($\geq 60°$), an increase in wind speed between 11–22 knots, and a short-term decrease in average air temperature potential (θ) of 2.0–6.0 K. These conditions align with criteria used to define the presence of a cold pool and significantly impact the safety of flight operations, particularly during the landing phase.

Radar imagery shows that the cold pool formed in conjunction with a convective cell with a sharp reflectivity gradient at its edge. CNN and Grad-CAM-based analyses confirmed that this area of reflectivity gradient was the primary focus of the model, which also physically corresponded to the presence of a gust front. These findings demonstrate that a machine learning-based approach can support the automatic detection of cold pools from radar imagery while providing interpretations consistent with an understanding of atmospheric dynamics.

In terms of vertical dynamics, the observed cold pools ranged in depth from 300 to 1450 meters with a median of 800 meters, propagation speeds of 4–5 m/s, and C^2 strength exceeding 100 m^2/s^2 in some cases. Furthermore, an increase in relative humidity of up to 30% at the edge of the cold pool indicates the important role of this phenomenon in triggering the formation of new convective clouds with lower bases. Thus, cold pools not only pose a direct threat to

aviation due to strong surface winds but also have the potential to strengthen surrounding convective systems.

Overall, this study confirms that cold pools are a significant meteorological phenomenon that requires greater attention in the context of flight operations at Soekarno–Hatta Airport. The combination of multi-instrument observations and a machine learning-based approach proved effective in identifying the characteristics of this phenomenon. Going forward, the results of this study can serve as the basis for the development of a more adaptive early warning system to minimize the risk of flight disruptions caused by cold pools.

Acknowledgments

The Authors would like to thanks to BMKG (Indonesian Meteorology Climatology and Geophysics Agency) especially to PPSDM (Center of Development in Human Resource) for fully funding this research.

References

Allen, C. J. T., Washington, R., & Engelstaedter, S. (2013). Dust emission and transport mechanisms in the central Sahara: Fennec ground-based observations from Bordj Badji Mokhtar, June 2011. *Journal of Geophysical Research: Atmospheres*, *118*(12), 6212–6232. https://doi.org/10.1002/jgrd.50534

Ashpole, I., & Washington, R. (2013). A new high-resolution central and western Saharan summertime dust source map from automated satellite dust plume tracking. *Journal of Geophysical Research: Atmospheres*, *118*(13), 6981–6995. https://doi.org/10.1002/jgrd.50554

Billings, B. J., Grubišić, V., & Borys, R. D. (2006). Maintenance of a Mountain Valley Cold Pool: A Numerical Study. *Monthly Weather Review*, *134*(8), 2266–2278. https://doi.org/10.1175/mwr3180.1

Borque, P., Nesbitt, S. W., Trapp, R. J., Lasher-Trapp, S., & Oue, M. (2020). Observational Study of the Thermodynamics and Morphological Characteristics of a Midlatitude Continental Cold Pool Event. *Monthly Weather Review*, *148*(2), 719–737. https://doi.org/10.1175/mwr-d-19-0068.1

Bou Karam, D., Williams, E., Janiga, M., Flamant, C., McGraw-Herdeg, M., Cuesta, J., Auby, A., & Thorncroft, C. (2014). Synoptic-scale dust emissions over the Sahara Desert initiated by a moist convective cold pool in early August 2006. *Quarterly Journal of the Royal Meteorological Society*, *140*(685), 2591–2607. https://doi.org/10.1002/qj.2326

Chen, Y.-C., Chang, T.-Y., Chow, H.-Y., Li, S.-L., & Ou, C.-Y. (2022). Using Convolutional Neural Networks to Build a Lightweight Flood Height Prediction Model with Grad-Cam for the Selection of Key Grid Cells in Radar Echo Maps. *Water*, *14*(2), 155. https://doi.org/10.3390/w14020155

Falk, N. M., & Van Den Heever, S. C. (2023). Environmental Modulation of Mechanical and Thermodynamic Forcing from Cold Pool Collisions. *Journal of the Atmospheric Sciences*, *80*(2), 375–395. https://doi.org/10.1175/jas-d-22-0020.1

James, R. P., Markowski, P. M., & Fritsch, J. M. (2006). Bow Echo Sensitivity to Ambient Moisture and Cold Pool Strength. *Monthly Weather Review*, *134*(3), 950–964. https://doi.org/10.1175/mwr3109.1

Kocha, C., Tulet, P., Lafore, J. -P., & Flamant, C. (2013). The importance of the diurnal cycle of Aerosol Optical Depth in West Africa. *Geophysical Research Letters*, *40*(4), 785–790. https://doi.org/10.1002/grl.50143

Lemon, L. R., & Doswell, C. A. (1979). Severe Thunderstorm Evolution and Mesocyclone Structure as Related to Tornadogenesis. *Monthly Weather Review*, *107*(9), 1184–1197. https://doi.org/10.1175/1520-0493(1979)107<1184: STEAMS>2.0.CO;2

Lensky, I. M., & Rosenfeld, D. (2008). Clouds-Aerosols-Precipitation Satellite Analysis Tool (CAPSAT). *Atmospheric Chemistry and Physics*, *8*(22), 6739–6753. https://doi.org/10.5194/acp-8-6739-2008

Li, Z., Zuidema, P., & Zhu, P. (2014). Simulated Convective Invigoration Processes at Trade Wind Cumulus Cold Pool Boundaries. *Journal of the Atmospheric Sciences*, *71*(8), 2823–2841. https://doi.org/10.1175/jas-d-13-0184.1

Mallinson, H. M., & Lasher-Trapp, S. G. (2019). An Investigation of Hydrometeor Latent Cooling upon Convective Cold Pool Formation, Sustainment, and Properties. *Monthly Weather Review*, *147*(9), 3205–3222. https://doi.org/10.1175/mwr-d-18-0382.1

Marsham, J. H., Hobby, M., Allen, C. J. T., Banks, J. R., Bart, M., Brooks, B. J., Cavazos-Guerra, C., Engelstaedter, S., Gascoyne, M., Lima, A. R., Martins, J. V., McQuaid, J. B., O'Leary, A., Ouchene, B., Ouladichir, A., Parker, D. J., Saci, A., Salah-Ferroudj, M., Todd, M. C., & Washington, R. (2013). Meteorology and dust in the central Sahara:

Observations from Fennec supersite-1 during the June 2011 Intensive Observation Period. *Journal of Geophysical Research: Atmospheres*, *118*(10), 4069–4089. https://doi.org/10.1002/jgrd.50211

McDonald, J. M., & Weiss, C. C. (2021). Cold Pool Characteristics of Tornadic Quasi-Linear Convective Systems and Other Convective Modes Observed during VORTEX-SE. *Monthly Weather Review*, *149*(3), 821–840. https://doi.org/10.1175/MWR-D-20-0226.1

Redl, R., Fink, A. H., & Knippertz, P. (2015). An Objective Detection Method for Convective Cold Pool Events and Its Application to Northern Africa. *Monthly Weather Review*, *143*(12), 5055–5072. https://doi.org/10.1175/mwr-d-15-0223.1

Ross, T. I. D., & Lasher-Trapp, S. (2024). On CCN Effects upon Convective Cold Pool Timing and Features. *Monthly Weather Review*, *152*(3), 891–906. https://doi.org/10.1175/mwr-d-23-0154.1

Selvaraju, R. R., Cogswell, M., Das, A., Vedantam, R., Parikh, D., & Batra, D. (2020). Grad-CAM: Visual Explanations from Deep Networks via Gradient-based Localization. *International Journal of Computer Vision*, *128*(2), 336–359. https://doi.org/10.1007/s11263-019-01228-7

Shi, J., Wang, P., Wang, D., & Jia, H. (2019). Radar-Based Automatic Identification and Quantification of Weak Echo Regions for Hail Nowcasting. *Atmosphere*, *10*(6), 325. https://doi.org/10.3390/atmos10060325

Tang, Z., Tian, E., Wang, Y., Wang, L., & Yang, T. (2021). Nondestructive Defect Detection in Castings by Using Spatial Attention Bilinear Convolutional Neural Network. *IEEE Transactions on Industrial Informatics*, *17*(1), 82–89. https://doi.org/10.1109/TII.2020.2985159

Tompkins, A. M. (2001). Organization of Tropical Convection in Low Vertical Wind Shears: The Role of Cold Pools. *Journal of the Atmospheric Sciences*, *58*(13), 1650–1672. https://doi.org/10.1175/1520-0469(2001)058<1650: ootcil>2.0.co;2

Weisman, M. L. (1992). The Role of Convectively Generated Rear-Inflow Jets in the Evolution of Long-Lived Mesoconvective Systems. *Journal of Atmospheric Sciences*, *49*(19), 1826–1847. https://doi.org/10.1175/1520-0469(1992)049<1826: TROCGR>2.0.CO;2

Yuan, Y., Wang, P., Wang, D., & Jia, H. (2018). An Algorithm for Automated Identification of Gust Fronts from Doppler Radar Data. *Journal of Meteorological Research*, *32*(3), 444–455. https://doi.org/10.1007/s13351-018-7089-7

Zheng, J., Zhang, J., Zhu, K., Liu, L., & Liu, Y. (2014). Gust front statistical characteristics and automatic identification algorithm for CINRAD. *Journal of Meteorological Research*, *28*(4), 607–623. https://doi.org/10.1007/s13351-014-3240-2